SEPT: TOWARDS EFFICIENT SCENE REPRESENTATION LEARNING FOR MOTION PREDICTION

Zhiqian Lan[1,*], **Yuxuan Jiang**[1,*], **Yao Mu**[2], **Chen Chen**[1], **Shengbo Eben Li**[1,†]
Hang Zhao[3], **Keqiang Li**[1]
[1]School of Vehicle and Mobility, Tsinghua University
[2]Department of Computer Science, The University of Hong Kong, [3]IIIS, Tsinghua University
{lanzq21, jyx21, chenchen20}@mails.tsinghua.edu.cn, ymu@cs.hku.hk
{lishbo, likq}@tsinghua.edu.cn, hangzhao@mail.tsinghua.edu.cn

ABSTRACT

Motion prediction is crucial for autonomous vehicles to operate safely in complex traffic environments. Extracting effective spatiotemporal relationships among traffic elements is key to accurate forecasting. Inspired by the successful practice of pretrained large language models, this paper presents SEPT, a modeling framework that leverages self-supervised learning to develop powerful spatiotemporal understanding for complex traffic scenes. Specifically, our approach involves three masking-reconstruction modeling tasks on scene inputs including agents' trajectories and road network, pretraining the scene encoder to capture kinematics within trajectory, spatial structure of road network, and interactions among roads and agents. The pretrained encoder is then finetuned on the downstream forecasting task. Extensive experiments demonstrate that SEPT, without elaborate architectural design or manual feature engineering, achieves state-of-the-art performance on the Argoverse 1 and Argoverse 2 motion forecasting benchmarks, outperforming previous methods on all main metrics by a large margin.

1 INTRODUCTION

Accurately predicting the future trajectories of surrounding road users is crucial to a safe and efficient autonomous driving system. In addition to kinematic constraints, the future motions of traffic agents may be shaped by many factors in the traffic scene, including shape and topology of roads, and surrounding agents' behaviors. Modeling and understanding these intricate relationships within the scene has long been a core challenge for motion prediction.

Researches in the early stage predominantly use rasterized semantic images to represent the whole scene from a top-down view, and fuse the information with convolutional neural networks (Lee et al., 2017; Chai et al., 2019; Phan-Minh et al., 2020). Due to the information loss during rasterization, recent researches have shifted to a vectorized paradigm in which the agents and roads are represented as a set of vectors. This representation has served as the foundation for numerous advanced methods that employ graph neural networks and transformers for scene encoding (Liang et al., 2020; Zhou et al., 2022). However, these prevailing SOTA methods typically embrace sophisticated architectural designs, which often rely on anchor-based modeling (Wang et al., 2022) or intermediate trajectory proposals (Wang et al., 2023b) to enhance the prediction performance. These empirical techniques consequently lead to an intricate and time-consuming information processing pipeline.

While previous attempts on scene encoding have focused on innovations in feature engineering and architectural design, we believe that the encoders built on universal architectures can develop strong comprehension on traffic scenes through a properly designed training scheme. A promising direction is to explore self-supervised learning (SSL). Large language models like GPT-3 (Brown et al., 2020) have leveraged SSL on large text corpora to learn broadly applicable linguistic knowledge, achieving significant advancement on a diverse set of NLP tasks. This inspires us that motion prediction

[*]Equal contribution.
[†]Correspondence to Shengbo Eben Li, email: lishbo@tsinghua.edu.cn

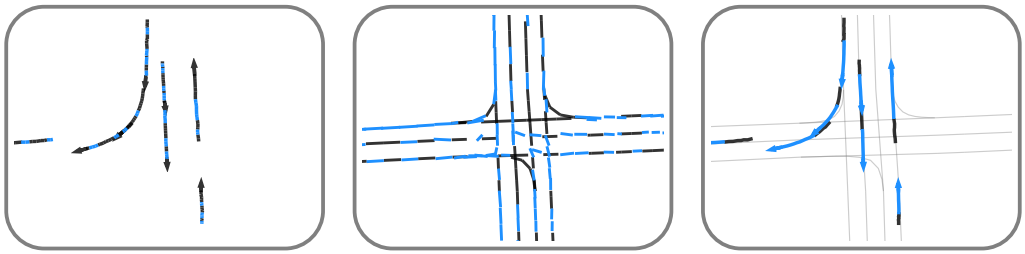

(a) MTM (b) MRM (c) TP

Figure 1: Illustration for our proposed scene understanding training tasks. For each picture, the masked or truncated scene inputs are painted in black while the corresponding reconstructed results are painted in blue.

models can implicitly be endowed with useful knowledge about traffic scenes such as environment dynamics and social interactions by effective self-supervised objectives.

Driven by this inspiration, we propose Scene Encoding Predictive Transformer (SEPT), a neat and powerful motion prediction framework that leverages SSL to progressively develop the spatiotemporal understanding for traffic scenes. We construct the self-supervised pretraining scheme for SEPT's scene encoder to capture three key aspects of scene context: temporal dependency within historical trajectory, spatial structure of road network, and interactions among roads and agents, yielding three corresponding pretraining tasks: Marked Trajectory Modeling (MTM), Masked Road Modeling (MRM), and Tail Prediction (TP). MTM, as shown in Figure 1a, randomly masks and reconstructs some waypoints in the agents' trajectories, to encode the temporal dependency arising from kinematic constraints. Similarly, MRM (Figure 1b) randomly masks some portion of the road vectors and then predicts the masked part, allowing the encoder to effectively capture the topology and connectivity of road network. While the previous two tasks handle single input modality, the third task TP (Figure 1c) focuses on interactions between modalities by conducting a short-term motion prediction task. In this task, we divide the agents' trajectories into two sections, named as head and tail, and the objective is to predict the tail section based on the preceding head section and the road context. The pretrained encoder is then finetuned to the downstream motion prediction task.

The effectiveness of the proposed SEPT are demonstrated by extensive experiments from two aspects. First, the model with pretraining achieves significant improvement over the model learned from scratch on all motion forecasting metrics consistently, showing that the model gains beneficial knowledge through pretraining objectives. Second, the three self-supervised pretraining tasks effectively collaborate with each other and yield positive effects on the final performance in an additive manner. Meanwhile, our experimental results on Argoverse 1 and Argoverse 2 datasets establish SEPT as a top-performing model, ranking 1st across all primary metrics on both large-scale motion forecasting benchmarks. Moreover, compared to the strongest baseline (Zhou et al., 2023) to our knowledge, our model achieves twice faster inference speed with only 40% network parameters.

2 Related Works

Scene encoding with transformers. Inspired by the remarkable success of transformer architecture, attention mechanism has been extensively used in motion prediction to model the long-range and complicated interactions within the traffic scene. Early attempts have only employed attention in specific sub-modules to encode spatial relationships such as agent social interactions (Tang and Salakhutdinov, 2019; Mercat et al., 2020; Salzmann et al., 2020). Recent SOTA approaches, on the other hand, tend to process all input modalities, including trajectories and road network, jointly with hierarchically stacked transformer blocks (Ngiam et al., 2021; Nayakanti et al., 2023; Zhou et al., 2023). These approaches represent the whole traffic scene as 3-D tensors (space-time-feature) and employ factored attention alternately along the temporal and spatial axes for several rounds to exploit spatiotemporal dependencies. Though sharing the same architectural design concept, the proposed SEPT adopts a more compact information processing pipeline, where temporal and spatial

information are encoded sequentially. This leads to a neat model architecture with fewer functional blocks.

Self-supervised learning in motion prediction. Some previous studies have explored self-supervised learning in motion prediction. To the best of our knowledge, the works most closely related to our research are Traj-MAE (Chen et al., 2023) and Forecast-MAE (Cheng et al., 2023). Following the idea of masked autoencoder (He et al., 2022), Traj-MAE randomly masks a portion of the input trajectories and road map, and utilizes the corresponding encoders to reconstruct the missing parts. However, a notable limitation of the method is that the spatial relationship between agents and roads are not stressed during pretraining since its trajectory and map encoder are trained separately, each with independent objectives. On the other hand, our SEPT introduces the Tail Prediction task to capture the spatiotemporal relationship in the traffic scene concurrently, and its effectiveness is proved in the experiments. The other work, Forecast-MAE, adopts a distinct masking strategy for agent trajectory. Notably, this approach incorporates the ground truth future trajectories of agents into its pretraining stage and predict the future given its history or vice versa. Whereas, not all self-supervisory tasks in Forecast-MAE contribute to the downstream prediction task positively. As is reported in its ablation study, several combinations of tasks may degrade the final performance compared to models learned from scratch. Instead, SEPT's ablation studies show that all task combinations could improve performance in a consistent and additive manner.

3 APPROACH

3.1 INPUT REPRESENTATION

SEPT represents the traffic scene input with the following modalities:

Agent trajectories are represented as a tensor $[A, T, D_h]$, which captures the recent trajectories of A nearest traffic agents relative to the target agent, including itself. Each agent's trajectory is represented as a time series of T state vectors, containing coordinates, timestamp, agent type, and any other attributes provided in the dataset. All position coordinates are transformed into the local coordinate system of the target agent at its T-th frame. In addition, not all agents have full T frames of history as the target agent. Shorter agent history is padded to T frames and properly masked for further attention computation.

Road network is represented as a set of R road vectors $[R, D_r]$, based on the vectorized map representation from VectorNet (Gao et al., 2020). Each road vector is a directed lane centerline segment with features including start and end positions, length, turn direction, and other semantics from the dataset. To obtain fine-grained inputs for the road network, lane centerlines are segmented into vectors spanning no longer than 5 meters in length. Representing the entire road network in this way results in an input vector set of massive scale, bringing excessive computational and memory burden in self-attention modules. SEPT introduces a *road pruning module* based on static path planning layer from Guan et al. (2022), to identify potential routes for the target agent within the predictive horizon and construct a more compact subset $[S, D_r]$.

3.2 MODEL ARCHITECTURE

Figure 2 illustrates the simple but expressive model architecture of the proposed SEPT. The model comprises an encoder for scene encoding and a decoder that predicts a weighted set of trajectories based on scene memory embeddings.

Projection layer projects different input modalities into a shared high dimensional vector space $\mathbb{R}^D$ in order to perform follow-up attention operations. A projection layer in SEPT is a single linear layer with ReLU activation, i.e., $\text{Project}(x) = \max(Wx + b, 0)$.

TempoNet consists of K_T stacked Transformer encoder blocks, and is used for agent history encoding. TempoNet takes as input agent history embeddings $[A, T, D]$ and conducts self-attention operation along temporal dimension T. After that, the embeddings across time steps are aggregated through max pooling to produce agent embeddings $[A, D]$. Additionally, TempoNet applies the simplified relative position embedding proposed in T5 (Raffel et al., 2020), to encode relative order of time steps.

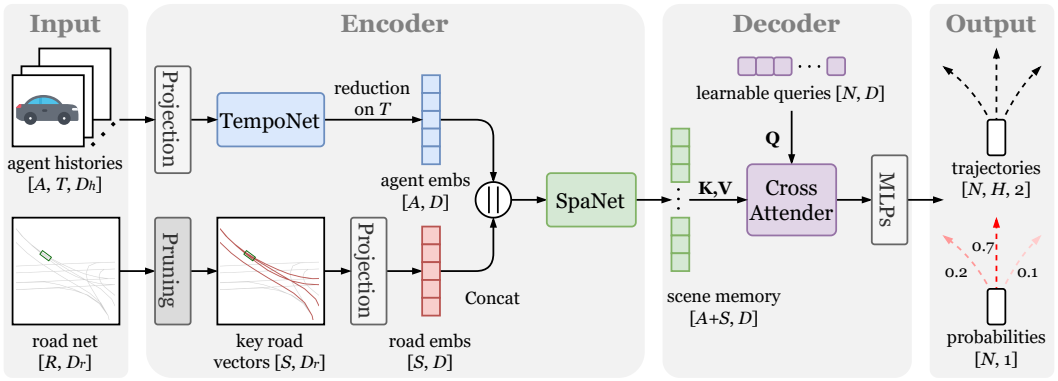

Figure 2: The overall architecture of SEPT

SpaNet concatenates K_S Transformer encoder blocks as TempoNet does, and its primary objective is to capture spatial relationships within the traffic scene. Its scene embedding input is formed by concatenating agent and road embeddings. Notably, compared to many previous SOTA methods, SEPT avoids the use of dedicated modules that separately encode agent interaction, road network, and agent-road relations. Instead, SpaNet leverage self attention across spatial dimension $A + S$ to fulfill these encoding objectives in a unified way.

Cross Attender comprises K_C stacked cross attention layers. This module cross attends a set of N learnable queries $[N, D]$ with the scene memory embeddings $[A + S, D]$ from the encoder. This generates N embeddings $[N, D]$ corresponding to the N output modalities. Each embedding vector is then mapped from the hidden space to the physical world through two MLPs, producing the predicted 2D trajectory and its associated confidence score.

3.3 Scene Understanding Training

In the scene understanding training stage, we train the encoder of SEPT to understand the temporal and spatial relationships in the traffic scene, and produce high quality latent representations for the downstream trajectory prediction task. This is achieved with three self-supervised mask-reconstruction learning tasks on TempoNet, SpaNet, and their alignment, as is shown in Figure 3. In this stage, the model is optimized with the summation of the three tasks' objectives.

3.3.1 Task 1: Masked Trajectory Modeling (MTM)

MTM targets TempoNet for understanding the temporal dependencies in agents' trajectories. As is shown in Figure 3a, we randomly substitute a certain ratio of frames with a learnable mask token for all eligible input trajectories. By eligible here, we refer to trajectories longer than a certain threshold, because too short trajectories are often of low quality, and may not be informative enough for the model to learn meaningful representations. For MTM and two more scene understanding tasks below, the hidden vectors are fed into a shallow MLP decoder to produce reconstruction vectors, and the objective function is defined as the masked L_2 loss between reconstruction and original vectors.

3.3.2 Task 2: Masked Road Modeling (MRM)

As is shown in Figure 3b, MRM shares a similar idea with MTM but it targets SpaNet to learn the spatial structure of road vector input. Different from the trajectories in MTM, road segments form a graph rather than a sequence, where simple positional encoding becomes unsuitable. Without bias about relative position information, learning with the token-level mask would be difficult, since a time consuming linear assignment problem needs to be solved to compute the reconstruction loss. We instead employ an attribute-level mask technique by setting all attributes, except for the coordinates of the starting point, to zero for selected road feature vectors. The starting point serves as a hint for SpaNet to reconstruct the original vectors. In doing so, SpaNet has to be aware of the

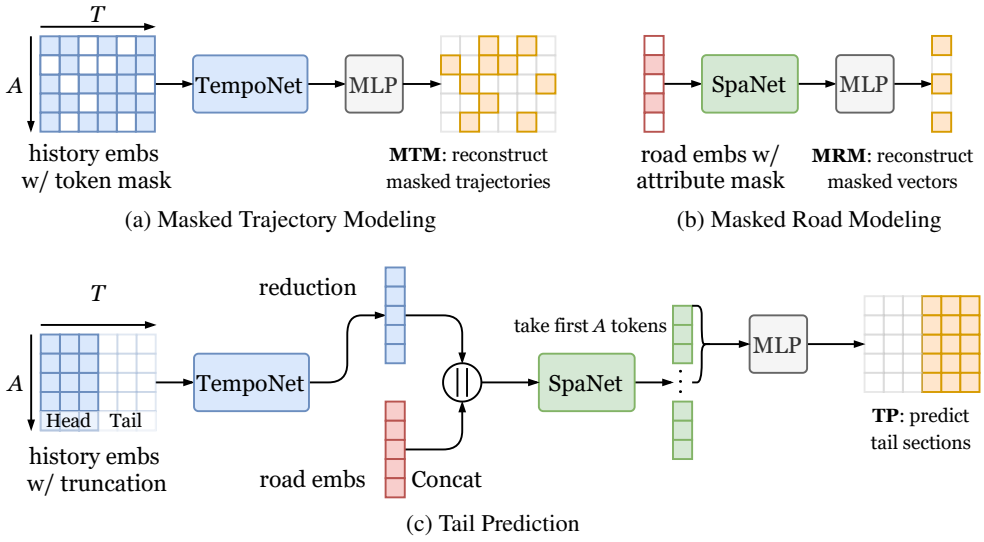

(a) Masked Trajectory Modeling (b) Masked Road Modeling

(c) Tail Prediction

Figure 3: SEPT tasks to learn the temporal and spatial relationship in the traffic scene

connectivity and continuity among unordered road vectors in order to recover the masked attributes like coordinates of endpoint.

3.3.3 Task 3: Tail Prediction (TP)

In TP, the agents' historical trajectories are divided into two sections along the trajectory axis: the head and the tail. The model is trained to predict the tail section given the head section by employing TempoNet and SpaNet jointly, which can be seen as a simplified version of motion prediction, as is shown in Figure 3c. Specifically, the agents' historical trajectories are truncated to the first T_h tokens before fed into TempoNet. Trajectories shorter than a threshold kT_h are excluded from prediction. Then, the embedding vectors of the truncated trajectories and the road embeddings are concatenated and fed into SpaNet. Finally, the hidden vectors of corresponding agents are fed into a shallow MLP decoder to predict the tail sections. This task is designed to align the trajectory representation learned in MTM with the road context representation learned in MRM and model their relationships, since accurate prediction requires effective use of both spatial and temporal information.

3.4 Motion Prediction Training

In the motion prediction training stage, we concatenate the pretrained encoder with the decoder, and train the whole model on the labeled dataset in an end-to-end fashion. For the motion prediction task, the loss function $\mathcal{L}$ consists of two terms: the trajectory regression loss $\mathcal{L}_{reg}$ and the classification loss $\mathcal{L}_{cls}$, which are defined in (1).

$$\begin{aligned} \mathcal{L} &= \mathcal{L}_{reg} + \mathcal{L}_{cls}, \\ \mathcal{L}_{reg} &= L_1 Loss(\tau_j, \tau_{gt}), \\ \mathcal{L}_{cls} &= -\sum_{i=1}^{N} \{\mathbb{I}(i=j)\log p_i + \mathbb{I}(i \neq j)\log(1-p_i)\}, \end{aligned} \tag{1}$$

where τ_i, p_i for $i = 1, \ldots, N$ are predicted trajectories with their normalized probabilities, and j refers to the index of the trajectory closest to ground truth in terms of average displacement error (ADE):

$$j = \arg\min_i ADE(\tau_i, \tau_{gt}).$$

Besides, $\mathbb{I}(\cdot)$ is the binary indicator function.

4 EXPERIMENTS

4.1 EXPERIMENTAL SETTINGS

Dataset. The effectiveness of our approach is verified on Argoverse 1 and Argoverse 2, two widely-used large-scale motion forecasting datasets collected from real world. The Argoverse 1 dataset consists of $324\,557$ driving scenarios, with each scenario contains 2-second historical context and 3-second future to predict. In contrast, the Argoverse 2 dataset comprises $250\,000$ scenarios, characterized by an extended 5-second historical context and a longer prediction horizon of 6 seconds. The trajectories in both datasets are sampled at $10\,\mathrm{Hz}$.

Metrics. Following the evaluation protocol used by Argoverse competition, we calculate the following metrics:

- **minFDE$_k$:** the l_2 distance between the endpoint of the best of k forecasted trajectories and the ground truth.
- **minADE$_k$:** the average l_2 distance between the best of k forecasted trajectories and the ground truth.
- **miss rate (MR$_k$):** the ratio of scenarios where minFDE$_k$ exceeds a threshold of $2\,\mathrm{m}$.
- **b-minFDE$_k$:** the minFDE$_k$ added by $(1.0 - p)^2$ where p is the probability of the best forecasted trajectory.

The best of k trajectories refers to the trajectory with its endpoint closest to ground truth endpoint. These metrics are calculated for $k = 6$ and $k = 1$, except for b-minFDE$_k$, which is only calculated for $k = 6$.

Training. In the scene understanding training stage, we remove labels (any trajectory frame after two seconds) from train, validation and test dataset, and concatenate those as the pretrain dataset. The model is trained for 150 epochs with a constant learning rate of 2×10^{-4}. In the downstream motion prediction training stage, we train and validate following the split of the Argoverse dataset. The model is trained for 50 epochs with the learning rate decayed linearly from 2×10^{-4} to 0. Both stages are trained with a batch size of 96 on a single NVIDIA GeForce RTX 3090 Ti GPU.

4.2 EXPERIMENTAL RESULTS

Comparison with baselines. We compare SEPT performance with SOTA published methods on the Argoverse 1 and Argoverse 2 leaderboards, including DenseTNT Gu et al. (2021), HOME Gilles et al. (2021), MultiPath++ Varadarajan et al. (2022), GANet Wang et al. (2023a), MacFormer Feng et al. (2023), DCMS Ye et al. (2023), Gnet Gao et al. (2023), Wayformer Nayakanti et al. (2023), ProphNet Wang et al. (2023b) and QCNet Zhou et al. (2023) , as is shown in Table 1 & 2.

Method	**b-minFDE$_6$**	minADE$_6$	minFDE$_6$	MR$_6$	minADE$_1$	minFDE$_1$	MR$_1$
DenseTNT	1.976	0.882	1.281	0.126	1.679	3.632	0.584
HOME	1.860	0.890	1.292	**0.085**	1.699	3.681	0.572
MultiPath++	1.793	0.790	1.214	0.132	1.624	3.614	0.565
GANet	1.790	0.806	1.161	0.118	1.592	3.455	0.550
MacFormer	1.767	0.812	1.214	0.127	1.656	3.608	0.560
DCMS	1.756	0.766	1.135	0.109	<u>1.477</u>	<u>3.251</u>	0.532
Gnet	1.751	0.789	1.160	0.117	1.569	3.407	0.545
Wayformer	1.741	0.768	1.162	0.119	1.636	3.656	0.572
ProphNet	1.694	0.762	1.134	0.110	1.491	3.263	0.526
QCNet	<u>1.693</u>	<u>0.734</u>	<u>1.067</u>	0.106	1.523	3.342	<u>0.526</u>
SEPT (Ours)	**1.682**	**0.728**	**1.057**	<u>0.103</u>	**1.441**	**3.178**	**0.515**

Table 1: Argoverse 1 leaderboard results sorted by b-minFDE$_6$. The best entry for a metric is marked bold, and the second best is underlined.

Method	**b-minFDE$_6$**	minADE$_6$	minFDE$_6$	MR$_6$	minADE$_1$	minFDE$_1$	MR$_1$
MacFormer	1.905	0.701	1.377	0.186	1.838	4.686	0.612
Gnet	1.896	0.694	1.337	0.180	1.724	4.398	0.588
ProphNet	1.882	0.657	1.317	0.179	1.764	4.768	0.610
QCNet	1.779	0.619	1.191	0.144	1.563	3.962	0.548
SEPT (Ours)	**1.736**	**0.605**	**1.151**	**0.137**	**1.485**	**3.700**	**0.545**

Table 2: Argoverse 2 leaderboard results.

On the Argoverse 1 dataset, our result outperforms all previous entries and ranks 1st on all metrics except for MR$_6$. For MR$_6$, HOME employs a "sparse sampling" technique to specialize miss rate performance while sacrifices other metrics. In this case, SEPT, being a general purpose method, ranks 2nd. Furthermore, for the Argoverse 2 dataset, SEPT consistently maintains its leading position on the leaderboard, ranking 1st on all metrics. Moreover, compared to QCNet, the strongest baseline in both benchmarks, SEPT has only 40% of its network parameters (around 9.6 million) while exhibits inference speed which is twice faster.

Comparison with related works. As is discussed in related works, Traj-MAE and Forecast-MAE share a similar idea of mask-reconstruction for trajectory prediction, but struggle to reach SOTA performance to justify pretraining. Traj-MAE reports minADE$_6$, minFDE$_6$ and MR$_6$ on Argoverse 1 test set, and Forecast-MAE reports these metrics on Argoverse 2 test set. As is shown in Table 3, SEPT outperforms these two methods by a large margin, further demonstrating our method's effectiveness.

Method	minADE$_6$	minFDE$_6$	MR$_6$
Traj-MAE	0.81	1.25	0.137
SEPT	**0.728**	**1.057**	**0.103**

(a) Comparison with Traj-MAE on Argoverse 1

Method	minADE$_6$	minFDE$_6$	MR$_6$
Forecast-MAE	0.690	1.338	0.173
SEPT	**0.605**	**1.151**	**0.137**

(b) Comparison with Forecast-MAE on Argoverse 2

Table 3: Performance comparison with related works

Trajectory prediction visualization. We compare the prediction results between the model with pretraining and the model trained from scratch in Figure 4. The visualization demonstrates that the model with pretraining can better capture the multimodality of driving purposes (shown in case 1) and generate the trajectories with improved conformity to road shapes (shown in case 2 & 3).

4.3 Ablation studies

The ablation studies focus on the scene understanding stage, specifically the effectiveness of various combinations of scene understanding tasks and the impact of their hyperparameters. We conduct ablation experiments following the same routine as the main experiment, and report the evaluation performance on the Argoverse 1 validation dataset. To minimize the impact of randomness, we conduct multiple experiments with different seeds for each configuration.

Effectiveness of scene understanding tasks. MTM, MRM and TP are three tasks introduced to learn a good prior for the downstream trajectory prediction task. To investigate the effectiveness, we conduct experiments for all 8 combinations, and the results are shown in Figure 5 and Table 4.

In Figure 5, we use solid lines for combinations involving task TP, and dashed lines for combinations without this task. It is clear that combinations with TP consistently outperform the opposites by learning faster at the beginning and performing better after convergence. This indicates that TP is effective to align TempoNet and SpaNet, therefore improve the overall representation quality of scene encoding. The other two tasks, MTM and MRM, can also improve performance in a consistent and additive manner. Furthermore, it should be noted that the configuration with all tasks active not only achieves the best performance, but also has the lowest variance over 5 runs among all combinations, as is shown in the shaded area in Figure 5. This suggests that our proposed

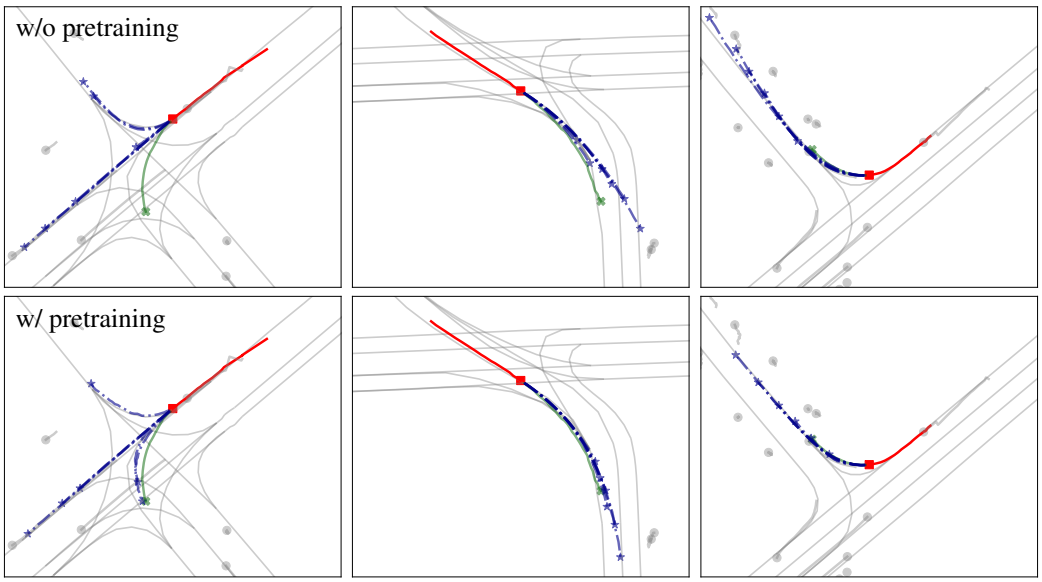

(a) case 1 (b) case 2 (c) case 3

Figure 4: Visualization results on three selected scenarios from Argoverse 1 validation set. The target agent's history and ground truth future are shown in red and green, respectively, while model's predictions are shown in blue. In each case, the upper image corresponds to the model that learns from scratch while the lower image corresponds to the model with scene understanding training.

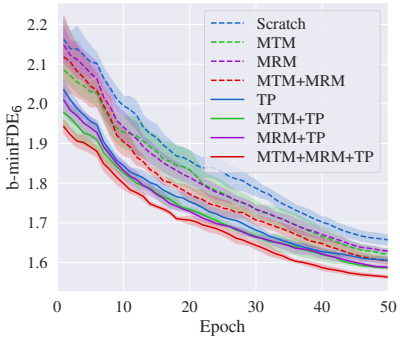

Task configuration			Final evaluation metrics			
MTM	MRM	TP	b-minFDE$_6$	minADE$_6$	minFDE$_6$	MR$_6$
			1.657	0.687	1.016	0.100
✓			1.620	0.670	0.980	0.095
	✓		1.628	0.674	0.988	0.096
✓	✓		1.603	0.663	0.964	0.091
		✓	1.605	0.661	0.964	0.091
✓		✓	1.586	0.653	0.947	0.089
	✓	✓	1.588	0.653	0.950	0.090
✓	✓	✓	**1.563**	**0.643**	**0.927**	**0.086**

Figure 5 & Table 4: The training curves report b-minFDE$_6$ performance for all task combinations. The solid or dashed lines correspond to the mean and the shaded regions correspond to 1-σ confidence interval over 5 runs. The table reports the final performance of all $k = 6$ metrics. The best entry for a metric is marked bold.

training approach can help the model converge to a good level consistently. Table 4 includes the final performance for all $k = 6$ metrics. It can be seen that other metrics exhibit similar patterns of improvement to b-minFDE$_6$ discussed above. Training curves for those metrics are included in the Appendix.

Effects of mask hyperparameters. In this ablation experiment, we show the impact of mask hyperparameters on final performance. For MTM and MRM, the main mask hyperparameter is the mask ratio p, implemented as sampling a mask from Bernoulli(p). For TP, the mask hyperparameter is the length of visible history T_h. For each of these three hyperparameters, we pretrain with the single corresponding task, then finetune with identical setting to get the final performance. As is shown in Figure 6, mask hyperparameters do not have a significant impact in suitable ranges and always outperform the model that trains from scratch. This suggests the effectiveness of our task design and

its robustness to choices of hyperparameters. In our main experiment, we simply use $p_{\text{MTM}} = 0.5$, $p_{\text{MRM}} = 0.5$ and $T_h = 8$ without tuning.

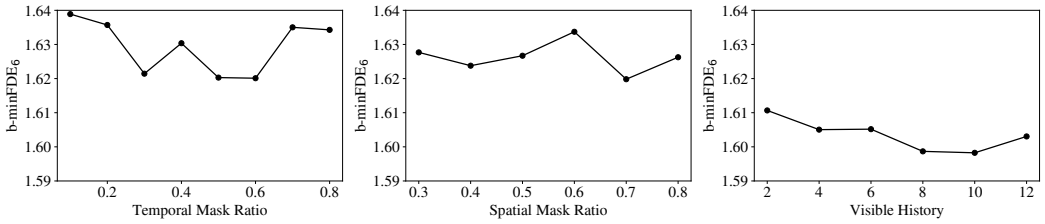

(a) MTM (b) MRM (c) TP

Figure 6: Final b-minFDE$_6$ performance of varying mask settings for each task, averaged over 5 runs.

5 Conclusion

In this paper, we present Scene Encoding Predictive Transformer (SEPT), a powerful modeling framework for accurate and efficient motion prediction. Leveraging three self-supervised mask-reconstruction learning tasks for scene understanding, we achieve SOTA performance on two large-scale motion forecasting datasets with a neat and unified model architecture. The ablation studies further demonstrate that introduced tasks can benefit final performance in a consistent and additive manner. Meanwhile, we acknowledge the limitation that, due to its agent-centric scene representation, SEPT is a single-agent prediction framework, and is not trivially extendable to multi-agent joint prediction. In the future, we will investigate further and generalize it to a more powerful multi-agent prediction framework.

References

Tom Brown, Benjamin Mann, Nick Ryder, Melanie Subbiah, Jared D Kaplan, Prafulla Dhariwal, Arvind Neelakantan, Pranav Shyam, Girish Sastry, Amanda Askell, et al. Language models are few-shot learners. *Advances in neural information processing systems*, 33:1877–1901, 2020.

Yuning Chai, Benjamin Sapp, Mayank Bansal, and Dragomir Anguelov. Multipath: Multiple probabilistic anchor trajectory hypotheses for behavior prediction. *arXiv preprint arXiv:1910.05449*, 2019.

Hao Chen, Jiaze Wang, Kun Shao, Furui Liu, Jianye Hao, Chenyong Guan, Guangyong Chen, and Pheng-Ann Heng. Traj-mae: Masked autoencoders for trajectory prediction, 2023.

Jie Cheng, Xiaodong Mei, and Ming Liu. Forecast-MAE: Self-supervised pre-training for motion forecasting with masked autoencoders. *Proceedings of the IEEE/CVF International Conference on Computer Vision*, 2023.

Chen Feng, Hangning Zhou, Huadong Lin, Zhigang Zhang, Ziyao Xu, Chi Zhang, Boyu Zhou, and Shaojie Shen. Macformer: Map-agent coupled transformer for real-time and robust trajectory prediction, 2023.

Jiyang Gao, Chen Sun, Hang Zhao, Yi Shen, Dragomir Anguelov, Congcong Li, and Cordelia Schmid. Vectornet: Encoding hd maps and agent dynamics from vectorized representation. In *Proceedings of the IEEE/CVF Conference on Computer Vision and Pattern Recognition*, pages 11525–11533, 2020.

Xing Gao, Xiaogang Jia, Yikang Li, and Hongkai Xiong. Dynamic scenario representation learning for motion forecasting with heterogeneous graph convolutional recurrent networks. *IEEE Robotics Autom. Lett.*, 8(5):2946–2953, 2023. doi: 10.1109/LRA.2023.3262150. URL `https://doi.org/10.1109/LRA.2023.3262150`.

Thomas Gilles, Stefano Sabatini, Dzmitry Tsishkou, Bogdan Stanciulescu, and Fabien Moutarde. HOME: heatmap output for future motion estimation. In *24th IEEE International Intelligent Transportation Systems Conference, ITSC 2021, Indianapolis, IN, USA, September 19-22, 2021*, pages 500–507. IEEE, 2021. doi: 10.1109/ITSC48978.2021.9564944. URL https://doi.org/10.1109/ITSC48978.2021.9564944.

Junru Gu, Chen Sun, and Hang Zhao. Densetnt: End-to-end trajectory prediction from dense goal sets. In *2021 IEEE/CVF International Conference on Computer Vision, ICCV 2021, Montreal, QC, Canada, October 10-17, 2021*, pages 15283–15292. IEEE, 2021. doi: 10.1109/ICCV48922.2021.01502. URL https://doi.org/10.1109/ICCV48922.2021.01502.

Yang Guan, Yangang Ren, Qi Sun, Shengbo Eben Li, Haitong Ma, Jingliang Duan, Yifan Dai, and Bo Cheng. Integrated decision and control: Toward interpretable and computationally efficient driving intelligence. *IEEE transactions on cybernetics*, 53(2):859–873, 2022.

Kaiming He, Xinlei Chen, Saining Xie, Yanghao Li, Piotr Dollár, and Ross Girshick. Masked autoencoders are scalable vision learners. In *Proceedings of the IEEE/CVF conference on computer vision and pattern recognition*, pages 16000–16009, 2022.

Namhoon Lee, Wongun Choi, Paul Vernaza, Christopher B Choy, Philip HS Torr, and Manmohan Chandraker. Desire: Distant future prediction in dynamic scenes with interacting agents. In *Proceedings of the IEEE conference on computer vision and pattern recognition*, pages 336–345, 2017.

Ming Liang, Bin Yang, Rui Hu, Yun Chen, Renjie Liao, Song Feng, and Raquel Urtasun. Learning lane graph representations for motion forecasting. In *Computer Vision–ECCV 2020: 16th European Conference, Glasgow, UK, August 23–28, 2020, Proceedings, Part II 16*, pages 541–556. Springer, 2020.

Jean Mercat, Thomas Gilles, Nicole El Zoghby, Guillaume Sandou, Dominique Beauvois, and Guillermo Pita Gil. Multi-head attention for multi-modal joint vehicle motion forecasting. In *2020 IEEE International Conference on Robotics and Automation (ICRA)*, pages 9638–9644. IEEE, 2020.

Nigamaa Nayakanti, Rami Al-Rfou, Aurick Zhou, Kratarth Goel, Khaled S. Refaat, and Benjamin Sapp. Wayformer: Motion forecasting via simple & efficient attention networks. In *IEEE International Conference on Robotics and Automation, ICRA 2023, London, UK, May 29 - June 2, 2023*, pages 2980–2987. IEEE, 2023. doi: 10.1109/ICRA48891.2023.10160609. URL https://doi.org/10.1109/ICRA48891.2023.10160609.

Jiquan Ngiam, Benjamin Caine, Vijay Vasudevan, Zhengdong Zhang, Hao-Tien Lewis Chiang, Jeffrey Ling, Rebecca Roelofs, Alex Bewley, Chenxi Liu, Ashish Venugopal, et al. Scene transformer: A unified architecture for predicting multiple agent trajectories. *arXiv preprint arXiv:2106.08417*, 2021.

Tung Phan-Minh, Elena Corina Grigore, Freddy A Boulton, Oscar Beijbom, and Eric M Wolff. Covernet: Multimodal behavior prediction using trajectory sets. In *Proceedings of the IEEE/CVF conference on computer vision and pattern recognition*, pages 14074–14083, 2020.

Colin Raffel, Noam Shazeer, Adam Roberts, Katherine Lee, Sharan Narang, Michael Matena, Yanqi Zhou, Wei Li, and Peter J Liu. Exploring the limits of transfer learning with a unified text-to-text transformer. *The Journal of Machine Learning Research*, 21(1):5485–5551, 2020.

Tim Salzmann, Boris Ivanovic, Punarjay Chakravarty, and Marco Pavone. Trajectron++: Dynamically-feasible trajectory forecasting with heterogeneous data. In *Computer Vision–ECCV 2020: 16th European Conference, Glasgow, UK, August 23–28, 2020, Proceedings, Part XVIII 16*, pages 683–700. Springer, 2020.

Charlie Tang and Russ R Salakhutdinov. Multiple futures prediction. *Advances in neural information processing systems*, 32, 2019.

Balakrishnan Varadarajan, Ahmed Hefny, Avikalp Srivastava, Khaled S. Refaat, Nigamaa Nayakanti, Andre Cornman, Kan Chen, Bertrand Douillard, Chi-Pang Lam, Dragomir Anguelov, and Benjamin Sapp. Multipath++: Efficient information fusion and trajectory aggregation for behavior prediction. In *2022 International Conference on Robotics and Automation, ICRA 2022, Philadelphia, PA, USA, May 23-27, 2022*, pages 7814–7821. IEEE, 2022. doi: 10.1109/ICRA46639.2022.9812107. URL https://doi.org/10.1109/ICRA46639.2022.9812107.

Jingke Wang, Tengju Ye, Ziqing Gu, and Junbo Chen. Ltp: Lane-based trajectory prediction for autonomous driving. In *Proceedings of the IEEE/CVF Conference on Computer Vision and Pattern Recognition*, pages 17134–17142, 2022.

Mingkun Wang, Xinge Zhu, Changqian Yu, Wei Li, Yuexin Ma, Ruochun Jin, Xiaoguang Ren, Dongchun Ren, Mingxu Wang, and Wenjing Yang. Ganet: Goal area network for motion forecasting. In *IEEE International Conference on Robotics and Automation, ICRA 2023, London, UK, May 29 - June 2, 2023*, pages 1609–1615. IEEE, 2023a. doi: 10.1109/ICRA48891.2023.10160468. URL https://doi.org/10.1109/ICRA48891.2023.10160468.

Xishun Wang, Tong Su, Fang Da, and Xiaodong Yang. Prophnet: Efficient agent-centric motion forecasting with anchor-informed proposals, 2023b.

Maosheng Ye, Jiamiao Xu, Xunnong Xu, Tengfei Wang, Tongyi Cao, and Qifeng Chen. Bootstrap motion forecasting with self-consistent constraints, 2023.

Zikang Zhou, Luyao Ye, Jianping Wang, Kui Wu, and Kejie Lu. Hivt: Hierarchical vector transformer for multi-agent motion prediction. In *Proceedings of the IEEE/CVF Conference on Computer Vision and Pattern Recognition*, pages 8823–8833, 2022.

Zikang Zhou, Jianping Wang, Yung-Hui Li, and Yu-Kai Huang. Query-centric trajectory prediction. In *Proceedings of the IEEE/CVF Conference on Computer Vision and Pattern Recognition (CVPR)*, pages 17863–17873, June 2023.

6 APPENDIX

6.1 RESULTS OF ABLATION STUDIES

Results of ablation studies for more evaluation metrics are shown in the following figures, which further corroborated the conclusions drawn in the main text.

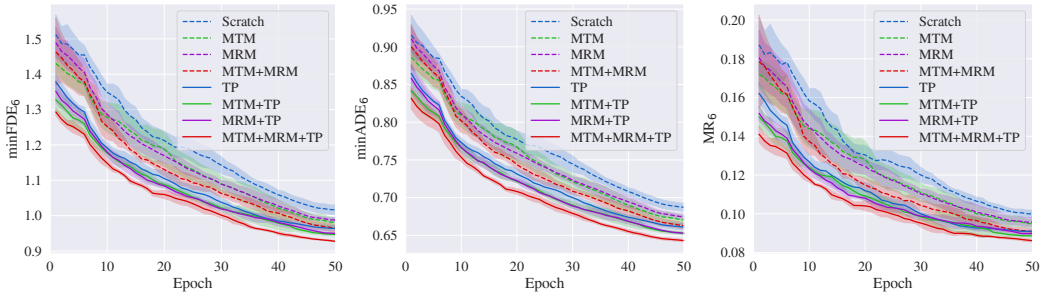

(a) minFDE_6 (b) minADE_6 (c) MR_6

Figure 7: The training curves report minFDE_6, minADE_6 and MR_6 performance of all task combinations. The solid or dashed lines correspond to the mean and the shaded regions correspond to 1-sigma confidence interval over 5 runs.

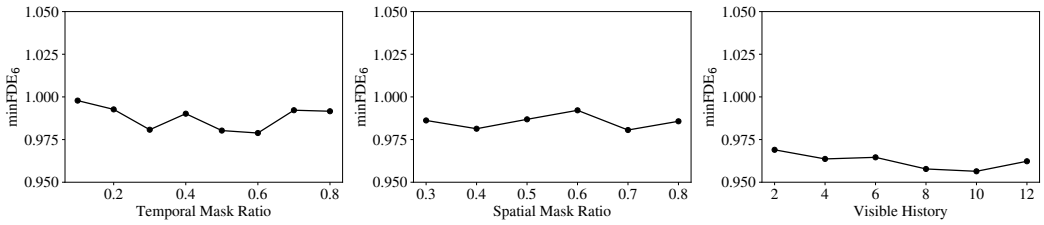

(a) MTM (b) MRM (c) TP

Figure 8: Final minFDE_6 performance of varying mask settings for each task, averaged over 5 runs.

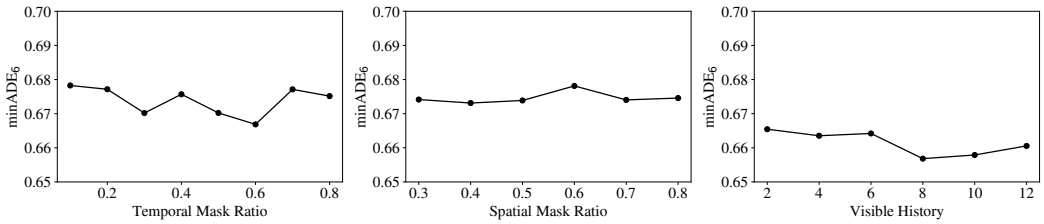

(a) MTM (b) MRM (c) TP

Figure 9: Final minADE_6 performance of varying mask settings for each task, averaged over 5 runs.

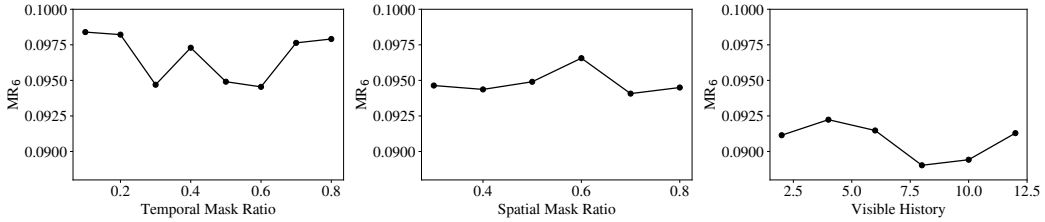

(a) MTM (b) MRM (c) TP

Figure 10: Final MR_6 performance of varying mask settings for each task, averaged over 5 runs.

6.2 HYPERPARAMETERS

Table 5 reports the hyperparameters for the SEPT network architecture. In all transformer layers, layer norm is done prior to attention and feedforward operations, and bias is cancelled in feedforward networks.

Arch	Parameters	Values
Projection	output size	256
TempoNet	depth	3
	num_head	8
	dim_head	64
SpaNet	depth	2
	num_head	8
	dim_head	64
Cross attender	depth	3
	num_head	8
	dim_head	64
	query size	256
MLP_traj	num_hidden	1
	hidden size	512
MLP_score	num_hidden	1
	hidden size	512

Table 5: Network hyperparameters